Dynamics of NO reduction by H_2 on Rh(111): Velocity and angular distributions of the N_2 product

J. I. Colonell, K. D. Gibson, and S. J. Sibener
The James Franck Institute and the Department of Chemistry, The University of Chicago, 5640 S. Ellis Avenue, Chicago, Illinois 60637

(Received 17 August 1995; accepted 17 January 1996)

The velocity and angular distributions of N_2 produced from the reduction of NO by H_2 on Rh(111) have been measured in the low nitrogen coverage limit as a function of surface temperature. Both the angular and velocity distributions are well fit by bimodal forms. The high energy channel has average translational energies about six times that expected for molecules accommodated at the surface temperature, an unusually sharp angular distribution, and angle dependent velocity distributions. The low energy channel is also hyperthermal, with average translational energies about twice thermal, a cosine angular distribution, and velocity distributions which are independent of angle. Application of surprisal analysis to the data shows that the high energy channel may be characterized by constraints on the normal velocity and the total energy; the low energy channel may be characterized by a single constraint on the velocity. © *1996 American Institute of Physics.* [S0021-9606(96)00116-X]

INTRODUCTION

Rhodium is included in three-way catalysts primarily for its ability to reduce nitric oxide and nitrogen oxide to nitrogen.[1,2] Platinum and palladium also catalyze the reduction of nitric oxide, but the primary products are ammonia and nitrous oxide rather than the desired N_2. The origin of the selectivity of rhodium catalysts for the formation of N_2 has been the subject of a great deal of study.[3] N_2 formation is also interesting as an example of a bimolecular surface reaction with a large barrier, an extremely important class of reactions which, though basic, are not yet fully understood.

Little is known about the dynamics of NO reduction on Rh(111). At low (room temperature thermal) energies N_2 does not dissociatively adsorb on rhodium,[4] so the dynamics of N_2 sticking and recombinative desorption are also unknown. In contrast, the dynamics of N_2 interactions with iron have been widely studied, due to their importance in ammonia synthesis.[5] N_2 sticking on Fe(111) is translationally activated with a barrier of $\sim$1–2 eV,[6] while vibrational energy does not promote the reaction.[7,8] The sticking coefficient is also temperature dependent, increasing with surface temperature, which suggests that the reaction occurs through a molecularly chemisorbed precursor.[6] N_2 dissociative adsorption on Re surfaces is also temperature dependent, and TPDs of N_2 recombinatively desorbing from Re(001) have a marked isotope effect.[9,10] Tunneling has been suggested to be important in the dynamics of N_2 interactions with both iron and rhenium surfaces.[11,12] The dynamics of N_2 sticking on tungsten surfaces have also been explored:[5] Direct activated adsorption with a barrier is seen on W(110)[13] and both activated and precursor-mediated channels are found on W(100).[14,15]

In this work, we examine the dynamics of the NO+H_2 reaction on the Rh(111) surface by measuring the velocity distribution of the product N_2 molecules as a function of desorption angle and surface temperature. Although the conditions are far from those of practical catalysts—ultrahigh vacuum and reducing conditions—these velocity distributions provide information about the potential energy surface (PES) governing the final step in the formation of N_2, a crucial element in a description of the catalytic activity of rhodium in this reaction.

Product velocity distributions have been measured for a number of surface reactions, and show a wide variety of angular and temperature dependencies.[16–29] In general, if there is no barrier in the final step of the reaction (e.g., desorption of a physisorbed molecule) angular distributions are expected to be roughly cosine and velocity distributions are expected to be similar to Maxwell–Boltzmann distributions at the surface temperature, T_s, with an average energy of $2k_bT_s$. Peaked angular distributions and average energies greater than $2k_bT_s$ are associated with energy barriers in the final step of the reaction.[30]

EXPERIMENT

These experiments were performed in a molecular beam scattering machine which has been described previously:[27,31,32] only the features essential to these experiments will be described in detail here. The UHV scattering chamber is pumped by a 400 ℓ/s ion pump and a TSP, contains a three-axis crystal manipulator, and an independently rotatable differentially pumped quadrupole mass spectrometer detector. Continuous beams of N_2 and hydrogen are produced by supersonic expansion in the source chamber. The beams are in a plane perpendicular to the scattering plane, one (the center beam) in the scattering plane defined by the plane of rotation of the detector, which can be chopped before the crystal, and the other (the side beam) inclined by 15°. The beam spots overlap at the crystal and are about 5 mm in diameter. The intensity of the side beam may be estimated from measurements of Ar beams in ion gauge

 0021-9606/96/104(17)/6822/12/$10.00

fluxmeters, and may be varied from about 10^{13} to 10^{14} s^{-1} (0.1 to 1 ML/s). The crystal may be moved out of the path of the center beam and the detector rotated to measure the velocity distribution of the incident beam directly.

A doubly differentially pumped post-crystal chopper is used to obtain the product velocity distributions. An ion pumped housing containing the motor (an ac hysteresis motor with high temperature windings), a small light bulb, and photodiode is bolted to the detector and rotates with it. A small slotted disk on one end of the motor shaft interrupts the light from the bulb which is detected by the photodiode to create the trigger signal. The other end of the motor shaft extends through a second ion pumped region into the scattering chamber, where the cross-correlation chopper is keyed to it. The chopper interrupts the product flux from the crystal 10.5 cm from the ionizer of the mass spectrometer.

The chopper pattern is a pseudorandom sequence of 511 slots and holes, and the wheel speed was 195.69 Hz, or a channel time of 10 μs. The N_2 TOF spectra were generally collected in 3×10^5–10^6 shots, or 15 min to 1 h of data collection. The surface was annealed at 1300 K after every 15 min of data collection to remove any oxygen absorbed in the bulk of the Rh crystal. The TOF spectra were fit by deconvolving them from the chopper pattern, and fitting the peak to a model function corrected for the velocity dependence of the ionization probability and convolved with the instrumental broadening due to the finite length of the ionizer.

The Rh(111) sample (Cornell Materials Preparation Lab) was cut and polished to within 1° of the (111) face and checked by x-ray Laue back reflection. The primary contaminants were S, B, and C. S and B were removed by cycles of Ar^+ sputtering (10 μA, 900 K) followed by annealing at 1300 K. C was removed daily by exposing the crystal to oxygen at 900 K and annealing at 1300 K. Oxygen absorbed into the bulk of the sample was removed by annealing the crystal at 1300 K for 3 min between measurements. Cleanliness was checked by Auger spectroscopy, and surface flatness by He reflectivity.

In all of these measurements, we used continuous beams of NO and H_2, with fluxes of $\sim10^{14}$/s ($\sim$1 ML/s) as estimated from fluxmeter measurements of Ar beams. The N atom coverage was measured by monitoring the N_2 intensity after the NO beam was turned off. The integral of this intensity was compared to the integrated H_2O signal from titrating a saturated (0.5 ML) oxygen overlayer with H_2. The ionization probabilities of N_2 and water are roughly equal;[33] the efficiency of the mass filter for the two species is assumed be similar. The surface coverage of oxygen was measured by titrating with H_2 after the NO beam was turned off. The coverages of NO and hydrogen could not be measured using these methods because they desorb too quickly. Estimating coverages from sticking coefficients and kinetic parameters determined from temperature programmed desorption measurements[34,35] yields $\sim10^{-5}$ ML for molecular NO and $\sim10^{-4}$ ML for hydrogen in the temperature range of these measurements (700–1000 K).

RESULTS

With NO and H_2 beams of $\sim10^{14}$ s^{-1} we measured N coverages less than 0.05 ML at all temperatures from 700 to 1000 K; the saturation coverage of nitrogen on Rh(111) when dosing with atomic nitrogen is $\sim$0.6 ML.[4] The oxygen coverages were also small, less than 0.1 ML. The TOF spectra, within our error, were not dependent on the NO beam intensity, suggesting that the coverage dependence of the dynamics is weak in this low N coverage regime.

The only products observed were N_2 and H_2O. We did not detect any NH_3 or N_2O. TOF spectra of the H_2O product produced in this reaction were found to be identical to those measured from the H_2+O_2 reaction, which suggests that the final step of water formation involved only the adsorbed oxygen atom, rather than the NO molecule. When the hydrogen beam is turned off, N_2 production rapidly decreases and becomes undetectable, perhaps because O atoms fill up the available sites for N adsorption and prevent NO dissociation.[36]

Typical N_2 TOF spectra are shown in Fig. 1. The surface temperature is 700 K and the fits are simply shifted Boltzmanns:

$$f(v)=Nv^3\,\exp\left[-\left(\frac{v-v_0}{\alpha}\right)^2\right]. \tag{1}$$

This form was chosen primarily for its flexibility: it varies smoothly from a Maxwell–Boltzmann distribution (with v_0 equal to zero and α equal to $\sqrt{(2k_bT_s)/(m)}$) to a narrow Gaussian typical of a supersonic beam. The TOF spectra become slower and broader at more glancing desorption angles, but never approach a Maxwell–Boltzmann at the surface temperature (shown by the dashed lines in Fig. 1).

There is no physical interpretation of the parameters of the shifted Boltzmann, but fitting the spectra allows them to be conveniently integrated to obtain the average energy and total intensity of the velocity distributions. The average energy near normal ($\theta_f=2°$) is shown as a function of temperature in Fig. 2. The dashed line shows the expected energy for molecules equilibrated at the surface temperature, that is,

$$\langle E\rangle=2k_bT_s, \tag{2}$$

the average energy of a Maxwell–Boltzmann distribution at the surface temperature. The energy of the product N_2 is nearly four times this value, and increases with a slope of $5.5k_b\pm1k_b$. The precision of the measurement of the average energy may be gauged from the scatter in the data which is about $\pm$30 meV; similar error bars should be assumed for all of the energy measurements. The accuracy of the energy measurement, that is, the calibration of the time of flight, was checked using effusive beams of He and O_2: These measurements suggested errors of less than 5 meV, much smaller than the scatter inherent in the current measurements, which is due to the low energy resolution at high energies. The angular dependence of the average energy is shown in Fig. 3.

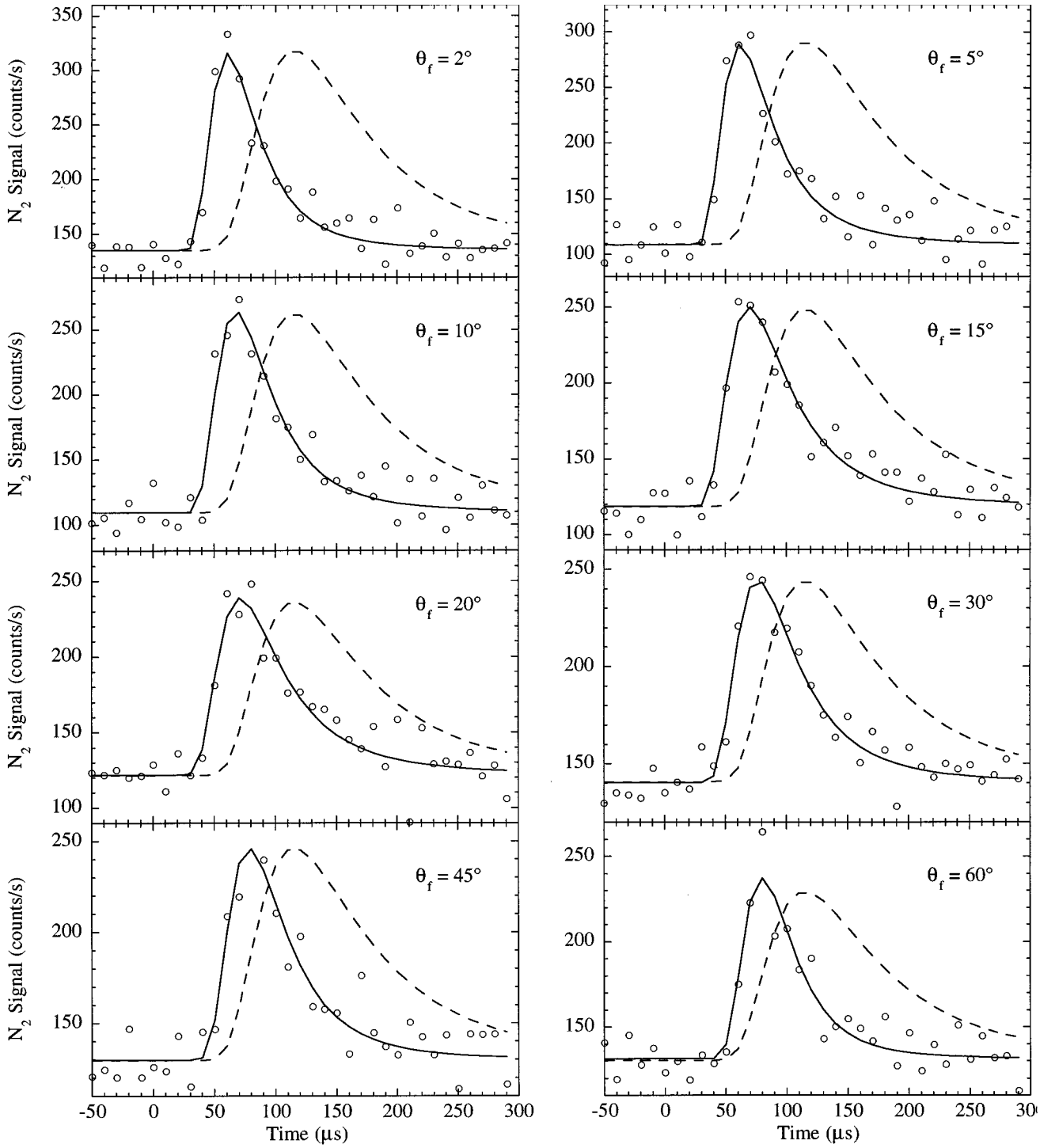

FIG. 1. TOF spectra at $T_s = 700$ K, deconvolved from the chopper function. The solid lines are fits to shifted Boltzmanns [Eq. (1)]; the dashed lines are Maxwell–Boltzmann distributions at the surface temperature.

The energy decreases rapidly at small desorption angles and approaches a constant value at glancing angles. However, even at 60°, the average energy is nearly twice that expected for molecules equilibrated at the surface temperature. The intensity decreases sharply with increasing desorption angle: Angular distributions measured at surface temperatures of 700 and 900 K are shown in Fig. 4. The angular distributions are best fit by the bimodal form

$$I(\theta_f) = a\ \cos^n(\theta_f) + (1-a)\cos(\theta_f), \tag{3}$$

where n is $\sim 25 \pm 5$, and is roughly constant with temperature. This is unusually sharp for an angular distribution, even for a reaction with a large barrier: For H_2 desorbing from Cu(111)[37,38] $n \sim 14$, while for CO_2 formed by oxidation of O on Rh and Pt,[21,39] $n \sim 9$. Only extremely energetic systems show such sharp angular distributions, e.g., N_2 formed by the

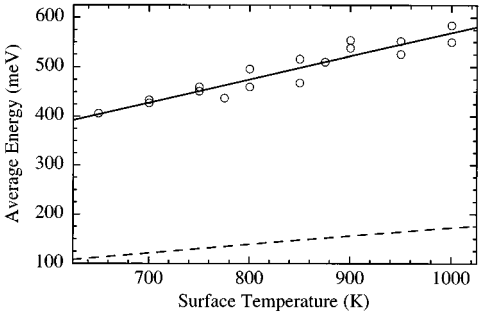

FIG. 2. Average energy of the N_2 desorbing at $\theta_f=2°$ as a function of surface temperature. The solid line is a linear fit to the data: $\langle E\rangle(\text{meV})=5.5(\pm1)k_bT_s+97(\pm50)$. The dashed line is Eq. (2), the expected energy for molecules equilibrated at the surface temperature.

decomposition of hydrazine,[40] for which $n\sim100$ and CH_4 formed by the photoinduced hydrogenation of CH_3 on Pt(111),[41] for which $n\sim30$. The second parameter, a, increases from ~0.4 to ~0.55 as T_s increases from 700 to 1000 K, that is, the fraction of the $\cos^n$ portion increases with increasing surface temperature.

The fact that the average energy becomes roughly independent of angle at large desorption angles coupled with the bimodal angular distributions suggests that the TOF distributions might also be bimodal. The observed angular dependence of the average energy suggests that the component which has a $\cos(\theta_f)$ angular distribution, and dominates at large desorption angles, has velocity distributions which are independent of desorption angle. The second component has a sharper angular distribution and higher energies, and its velocity distributions are angle dependent. The resulting form of the TOF spectrum is

$$f(v)=N(\theta_f)v^3\exp\left[-\left(\frac{v-v_0(\theta_f)}{\alpha(\theta_f)}\right)^2\right]+\left[\frac{\cos(\theta_f)}{\cos(60)}\right]f_{60}(v), \tag{4}$$

where $f_{60}(v)$ is simply a shifted Boltzmann fit to the data at 60°. Fits to this form of TOF spectra taken at a surface temperature of 900 K are shown in Fig. 5. The average energies of the high energy peak at 2° and the low energy peak, which

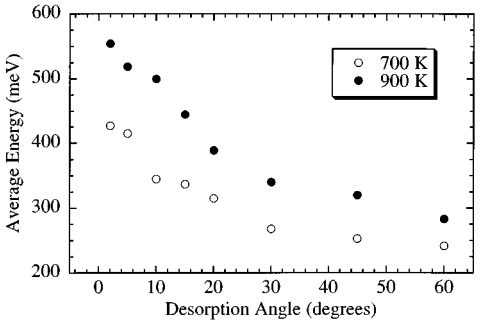

FIG. 3. Desorption angle dependence of the average energy. Open circles: $T_s=700$ K; filled circles: $T_s=900$ K.

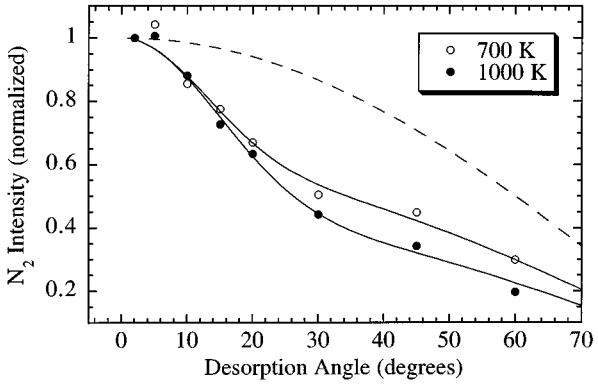

FIG. 4. Angular distribution of the intensity of desorbing N_2. Open circles: $T_s=700$ K; filled circles: $T_s=1000$ K. The solid lines are fits to Eq. (3) and the dashed line is $\cos(\theta_f)$.

is assumed to be independent of desorption angle, are shown as a function of temperature in Fig. 6. For both, the energy increases with a slope of $\sim2k_bT_s$. The average energy of the high energy peak is shown as a function of angle in Fig. 7: It decreases with increasing desorption angle. The two peaks may be integrated over all angles to yield the relative intensities of the two channels: The ratio of the high energy to the low energy N_2 is shown as a function of temperature in Fig. 8.

DISCUSSION

The adsorption and decomposition of NO has been studied on a variety of Rh surfaces.[34,36–48] The kinetics of the reduction of NO by H_2 and CO have also been studied on Rh[3,49–57] and PtRh[3,58–60] alloy surfaces, and show a rich variety of behaviors, from oscillations in reaction rates and selectivities to square chemical waves. The reaction mechanism for the reduction of NO by H_2 in the absence of ammonia formation is believed to be[58]

$$NO_{(g)}\leftrightarrow NO_{(ad)}, \tag{5}$$

$$H_{2(g)}\leftrightarrow 2H_{(ad)}, \tag{6}$$

$$NO_{(ad)}\rightarrow N_{(ad)}+O_{(ad)}, \tag{7}$$

$$2H_{(ad)}+O_{(ad)}\rightarrow H_2O_{(g)}, \tag{8}$$

$$N_{(ad)}+N_{(ad)}\rightarrow N_{2(g)}, \tag{9}$$

$$N_{(ad)}+NO_{(ad)}\rightarrow N_{2(g)}+O_{(ad)}. \tag{10}$$

One of the unsettled questions concerning this mechanism is the relative importance of reactions (9) and (10). The two channels were originally proposed in the mechanism of N_2 formation in temperature programmed desorption spectra of NO on polycrystalline rhodium by Campbell and White.[43] They observed two peaks in the N_2 TPD spectra which they suggested could be due to the operation of these two mechanisms for nitrogen formation. Root and Schmidt[36] also observed two peaks in the TPD of NO on Rh(111) and interpreted them in the same way, assigning the low temperature ($\sim$450 K) peak to reaction (10) and the high tem-

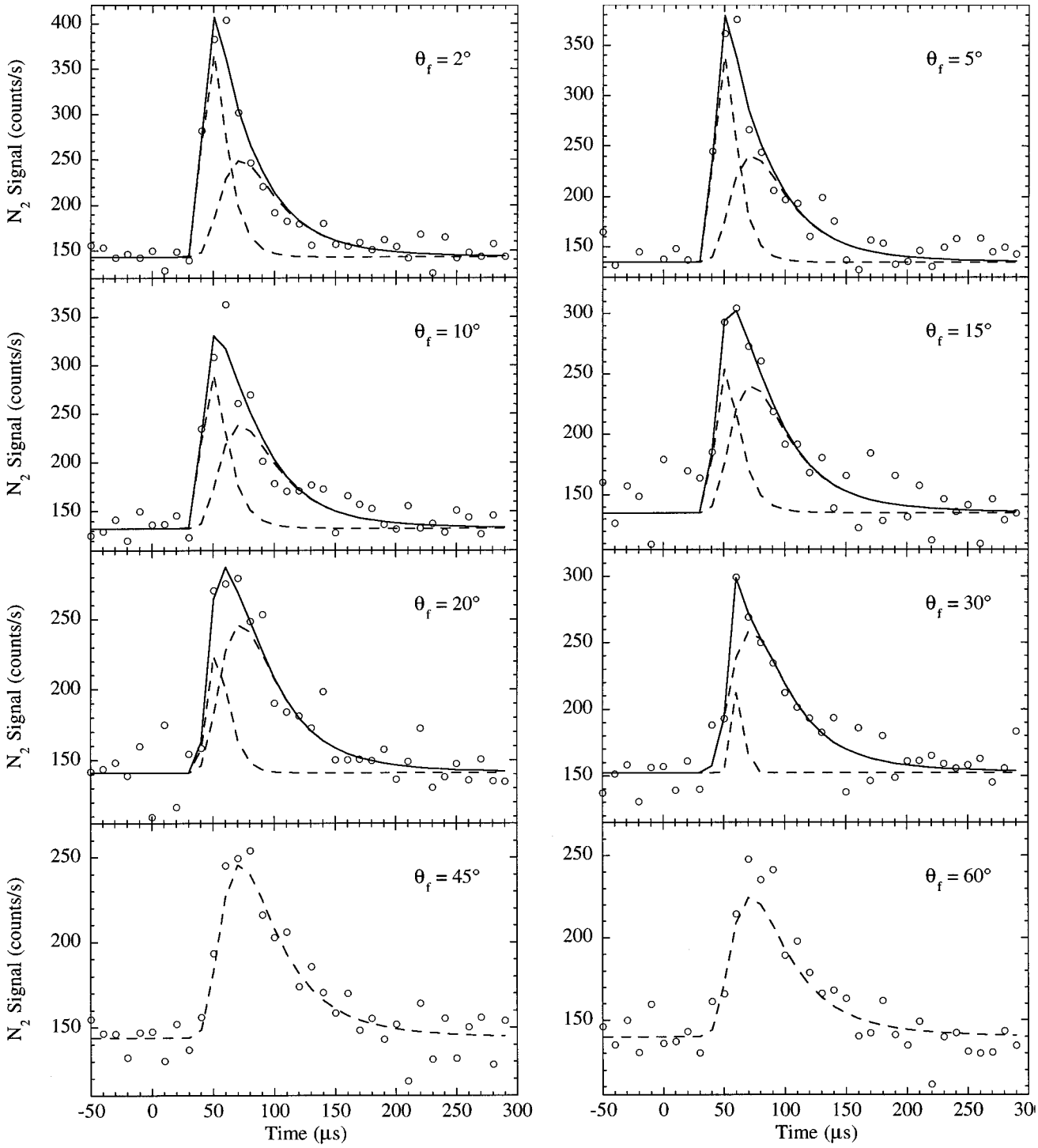

FIG. 5. Fits of TOF spectra at 900 K to the bimodal form in Eq. (4). The dashed lines show the decomposition into a high energy $\cos^n(\theta_f)$ distributed component and the $\cos(\theta_f)$ distributed component which is independent of angle. The solid line shows the sum.

perature (~700 K at low coverages) to reaction (9). However, Bugyi and Solymosi[4] have since measured TPD spectra of N_2 desorbing from Rh(111) dosed with atomic nitrogen and found they are identical to those from NO dosed Rh(111).[34] Therefore, the reaction of adsorbed NO with N to form N_2 is not seen in TPDs of NO on this surface.

The more relevant situation, however, is the reaction of NO and H_2 under steady state conditions at high surface temperatures. Obuchi *et al.*[52] measured the kinetics of NO reduction by hydrogen on Rh foil and also measured TPD spectra of recombining N atoms accumulated on the surface during the reaction. They found that the kinetics of N_2 formation during the steady state reaction and during the N_2 TPDs were the same, and concluded that N_2 formation proceeds by the same mechanism in the two cases, though recombination of nitrogen atoms. They also studied the kinet-

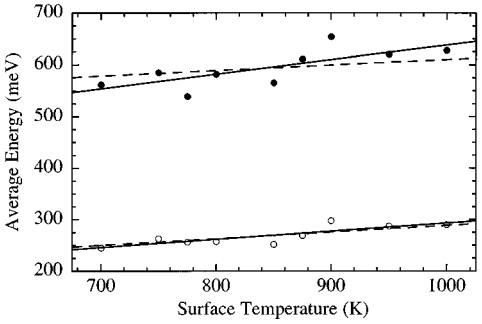

FIG. 6. Temperature dependence of the average energy of the two peaks. The filled circles are the average energy of the high energy peak at $\theta_f=2°$. The solid line is a linear fit to these points: $\langle E\rangle$(meV) $=3.3(\pm1)k_bT_s+350(\pm90)$. The open circles show the average energy of the low energy peak. The solid line is a fit to these data: $\langle E\rangle$(meV)$=1.9(\pm1)k_bT_s+130(\pm60)$. The dashed lines are fits to the van Willigen model.

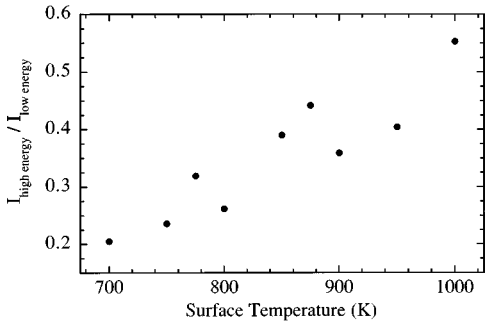

FIG. 8. Ratio of intensities of the high energy and low energy components of the TOF distribution, integrated over desorption angle, as a function of surface temperature.

ics of N_2 formation during the decomposition of NH_3, and found that it, too, had the same kinetics, supporting their conclusion. Reaction (10) has been shown to be significant on PtRh surfaces at high NO pressures and low temperatures ($<$500 K);[58] N_2O is a major product in the reaction of CO and NO on Rh(111) at high pressures,[49] so the reaction of NO and N may also occur on Rh(111). In short, both channels may be active under our reaction conditions, but since the surface temperature is relatively high, and the NO pressure low, nitrogen atom recombination is expected to dominate.

The overall reduction of NO to N_2 and water is exothermic by 79 kJ/mol (820 meV). However, the energetics which affect the dynamics of N_2 formation are those of reactions (9) and (10) in the mechanism outlined above, particularly reaction (9), the recombinative desorption of two adsorbed nitrogen atoms. The excess energy of a newly formed N_2 molecule (E_{total}) is

$$E_{\text{total}}=E_{\text{activation}}-\Delta H_{\text{reaction}}=E_{\text{activation}}-E_{\text{adsorption}}(N_2). \tag{11}$$

$E_{\text{adsorption}}(N_2)$ is the heat of dissociative adsorption, and, following convention, is positive if the adsorption is exothermic. $\Delta H_{\text{reaction}}$ is the enthalpy change for desorption, and is positive if the process is endothermic. Unfortunately, the energy of dissociative adsorption of N_2 on Rh(111) is unknown—when there is a barrier to adsorption, TPD measurements yield an estimate of the activation energy, not of $E_{\text{adsorption}}$. Bugyi *et al.*[4] found an activation energy of 205 kJ/mol (2100 meV) from their low coverage N_2 TPDs. Assuming that the adsorption of N_2 on Rh(111) is exothermic, this provides an upper limit on the total energy available for partitioning among the modes of the product N_2 molecule and the surface.

Essentially nothing is known about the energetics of the reaction of adsorbed NO and nitrogen atoms. Again, the binding energy of the nitrogen atom is unknown. The activation energy for the reaction has not been measured even on PtRh surfaces where it is known to occur, since it is difficult to study it independently from nitrogen atom recombination.

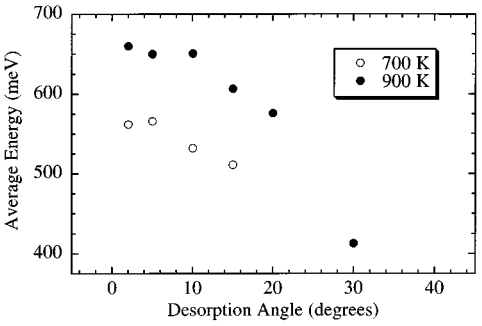

FIG. 7. Average energy of the high energy peak as a function of desorption angle. $T_s=700$ K: filled circles: $T_s=900$ K.

Origin of the bimodality

One possibility for the two channels observed in the angular and velocity distribution is that they represent reactions (9) and (10) in the reaction mechanism suggested. This question can only be decided by measuring the corresponding velocity distributions for N_2 recombination in the absence of NO. Unfortunately, neither N_2 nor NH_3 decomposes on Rh(111),[4,61] so a source of atomic N or, perhaps, excited N_2 is necessary for this definitive experiment. It is important to note, however, that it is also possible that the two peaks represent two channels of N_2 recombination. As mentioned earlier, there are two peaks in the N_2 TPDs: If the second peak is due to a second adsorption site (instead of nitrogen atom islands, or some other state which is only accessible at high coverages) the two peaks could correspond to the two peaks seen in the velocity distributions. Another possibility is that the two channels correspond to different vibrational states of the product N_2. Since the transition state for the reaction is likely an elongated N_2 molecule parallel to the surface, the PES for desorption into a vibrationally excited N_2 molecule might be expected to be considerably different than for desorption into the vibrational ground state.

Temperature and angular dependence of the average energy

Apart from detailed molecular dynamics simulations, which require a calculation of the entire PES for the reaction, most dynamical models of surface reactions are based on the idea of one dimensional barriers, or a distribution of one dimensional barriers. The earliest and simplest of these is the van Willigen model,[62] which assumes a single barrier perpendicular to the surface normal: Only molecules with enough ''normal energy'' overcome the barrier and desorb. The temperature dependence of the average energy of both channels may be fit fairly well with this model, with barrier heights of 350 meV for the high energy channel and 130 meV for the low energy channel (dashed lines in Fig. 6). However, the model also predicts a sharp cutoff in the TOF spectra at the barrier height which we do not see for either

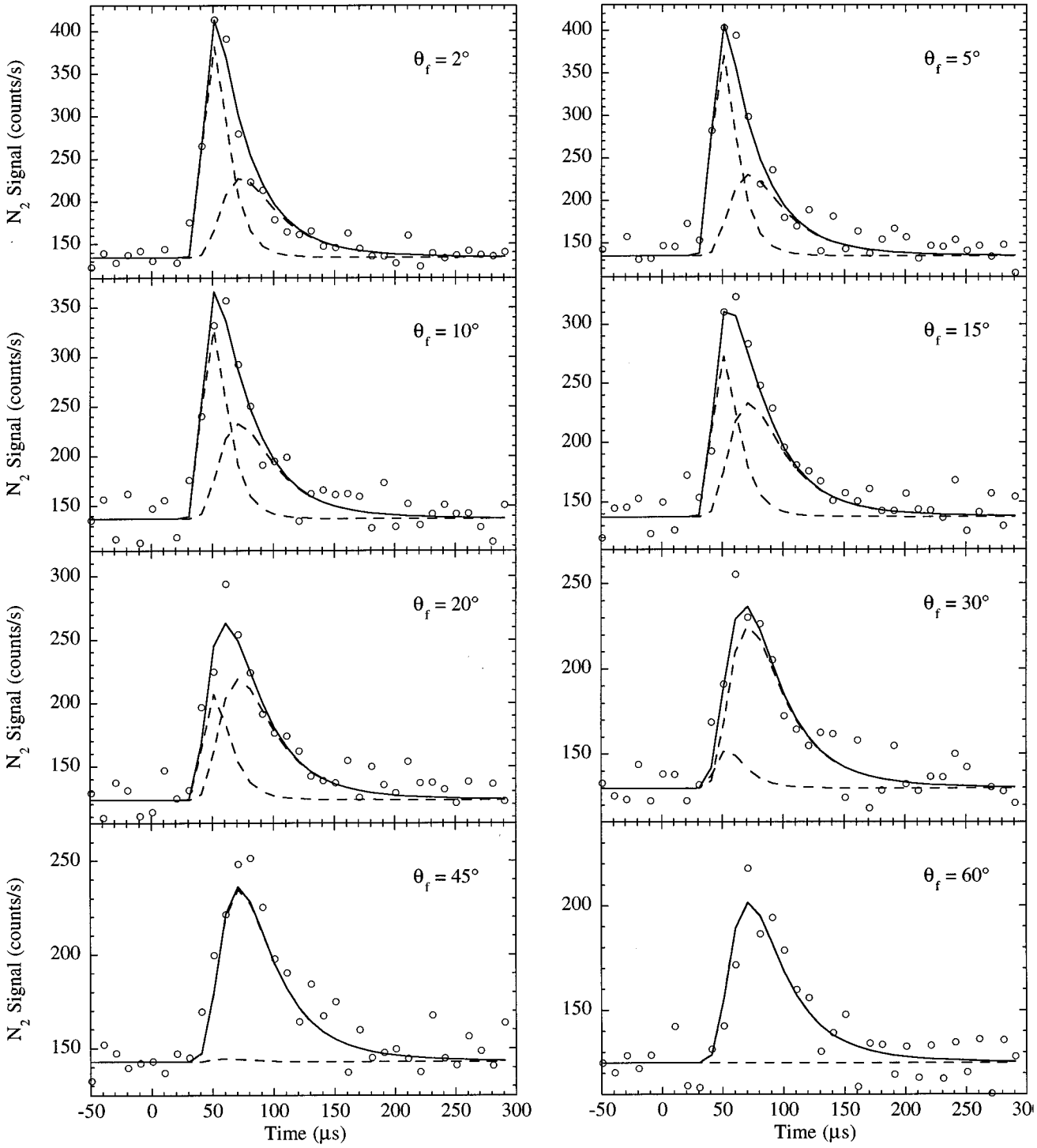

FIG. 9. TOF spectra at $T_s = 1000$ K fit to the surprisal form in Eq. (15).

channel. Also, the predictions for the angular dependence of both the energy and the intensity are incorrect. According to this model, the sharply peaked angular distribution of the high energy peak should correspond to a barrier height of 600 meV, and the energy should increase sharply with increasing desorption angle. Similarly, the $\cos(\theta_f)$ angular distribution of the low energy peak would correspond to a barrier height of zero.

Another version of the single one-dimensional barrier model was suggested by Doyen,[63] with important refinements by Verheij *et al.*[19] and Anger *et al.*[64] It relates the energy of the desorbing molecules to the angular distribution using a simple model for the interaction of the desorbing molecules with the surface phonons. This model predicts that the average energy scales with the sharpness of the angular distribution. For the $\cos^{25}(\theta_f)$ distribution of the high energy peak, it predicts an average energy of $14k_bT_s$, while for the $\cos(\theta_f)$ distribution of the low energy peak, it predicts an average energy of $2k_bT_s$.

Surprisal analysis

Given that the actual potential energy surface has at least 6 degrees of freedom, it is not surprising that a one dimensional model might not be able to account for all aspects of the dynamics. However, when only two of those degrees of freedom are being measured it is actually unlikely that all of the degrees of freedom need to be included in a model which accounts for the data. A standard method for constructing a model with the minimum number of parameters is surprisal analysis, which has been used extensively in gas phase dynamics,[65] and has also proved useful in analyzing the dynamics of surface reactions.[27,66,67] Surprisal analysis has been discussed at length elsewhere,[68–72] so only the primary result will be stated here.

The functional form for the ''most random'' possible distribution subject to some (small) number of constraints is

$$f_m(i)=f_0(i)\exp\left[-\sum_n \lambda_n A_n(i)\right], \tag{12}$$

where $f_m(i)$ is the measured distribution, the λ_n are the surprisal parameters, the A_n are the constrained variables, and $f_0(i)$ is the ''prior'' distribution, the most random possible distribution in the absence of any constraint. Another useful quantity is the information content of the distribution, or ''surprisal'' which is defined

$$I(i)=-\ln\left[\frac{f_m(i)}{f_0(i)}\right]=\lambda_1 A_1+\lambda_2 A_2+\cdots . \tag{13}$$

If a particular measured distribution can be defined by a single parameter, a plot of its surprisal vs i will be linear.

To apply surprisal analysis, one must choose a prior distribution and make an educated guess about the constraints. For the case of molecules desorbing from a surface, a logical choice for the prior distribution is that which arises from ''equilibrium'' desorption, where the desorbing molecules have accommodated at the surface temperature,

$$f_0(v)=Nv^3\cos(\theta_f)\exp\left(\frac{-mv^2}{2k_bT_s}\right). \tag{14}$$

Surprisal analysis of the high energy peak

In the case of the high energy peak, the high energies indicate a constraint on the velocity or energy. However, surprisal plots of the velocity distributions using either of these constraints are nonlinear, suggesting that more than one parameter is required to describe the velocity distributions. The sharply peaked angular distribution indicates a constraint on the desorption angle, probably either on the normal velocity or the normal energy. Surprisal plots of the angular distributions were found to be linear for both constraints: The angular range is not large enough to distinguish between $\cos(\theta_f)$ and $\cos^2(\theta_f)$, but one or the other is the key constraint on the angular distribution. Thus we tried combinations of constraints on the normal velocity, normal energy, total velocity, and total energy. The form which we found fit the velocity distributions at all desorption angles is [to make the sign of λ_1 positive, the sign of the surprisal parameters has been changed from Eqs. (12) and (13)]

$$f(v,\theta_f)=N_1 f_0(v,\theta_f)\exp[\lambda_1 v\cos(\theta_f)+\lambda_2 v^2] + N_2\left[\frac{\cos(\theta_f)}{\cos(60)}\right]f_{60}(v), \tag{15}$$

where $f_{60}(v)$ is the same shifted Boltzmann as in Eq. (4). λ_1, λ_2, N_1 and N_2 are not functions of the desorption angle, so all of the velocity distributions of the high energy peak at all desorption angles are fit with just four parameters. TOF spectra at 1000 K with fits to Eq. (15) are shown in Figs. 9. The temperature dependence of the surprisal parameters is shown in Fig. 10.

The physical meaning of the constraints may be interpreted using detailed balance, although the conclusions must be treated with caution, since measurements are made far from equilibrium and the effects of the internal state distributions are completely unknown. In general, at equilibrium, the sticking coefficient as a function of velocity and incident angle is given by

$$s(v,\theta_f)=\frac{\text{velocity distribution of desorbing molecules}}{\text{velocity distribution of a gas at } T_s \text{ incident on the surface}} \tag{16}$$

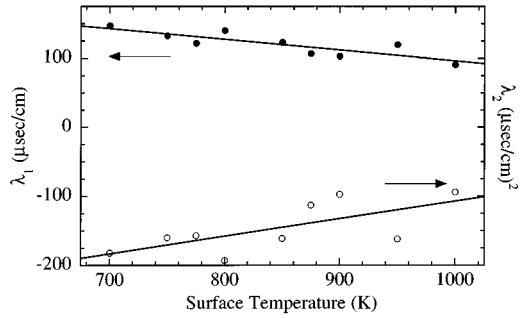

FIG. 10. Temperature dependence of the surprisal parameters used to fit the high energy peak.

which, for the high energy peak becomes

$$s(v,\theta_f) \propto \exp[\lambda_1 v\ \cos(\theta_f) + \lambda_2 v^2]. \tag{17}$$

It is important to realize that this form only applies for the energy range probed at a particular temperature, which may be determined from the range of energies seen in the measured velocity distributions: about 200–900 meV at 700 K and 200–1050 meV at 1000 K. Thus although the expression in Eq. (17) is not monotonic over all values of v (since λ_1 and λ_2 have opposite signs), the sticking coefficient is monotonic over the velocity range observed at these temperatures. The negative values of λ_2 cause the sticking coefficient to increase more slowly with normal velocity than a simple constraint on the velocity.

The temperature dependence of the surprisal parameters could be due to at least two causes. The most straightforward is that the energy dependence of the reaction probability changes as the temperature changes. A second possibility is that different energy ranges are probed at different temperatures, and that the dependence of $s(v,\theta_f)$ is somewhat different at different energies. If this is the case, we can patch together $s(v,\theta_f)$ over the whole energy range from sticking coefficients measured at different temperatures, as shown in panel (a) of Fig. 11. The solid line is $s(v,0°)$ at 700 K and the dashed line is $s(v,0°)$ at 1000 K, calculated from the surprisal parameters from the line fits in Fig. 10. The absolute values of the sticking coefficients are not known: We have no way of measuring the proportionality constant in Eq. (17), and the sticking coefficients have been arbitrarily set equal at $v=0.25$ cm/μs. The dashed vertical line shows the top of the velocity range measured at 700 K (99% of the intensity of the velocity distribution measured at 700 K and a desorption angle of 2° is below this value). The curves are quite similar below that point, but above it the 700 K curve is much too steep to fit the data at 1000 K. What Fig. 11(a) shows is that a single $s(v,\theta_f)$ could fit the data across the whole temperature range, but that curve will have a more complicated form than Eq. (17). Although temperature dependence of the dynamics can not be ruled out, the strong dependence of the reaction probability on normal velocity suggests that the molecule does not interact much with the surface during the reaction, since that would tend to

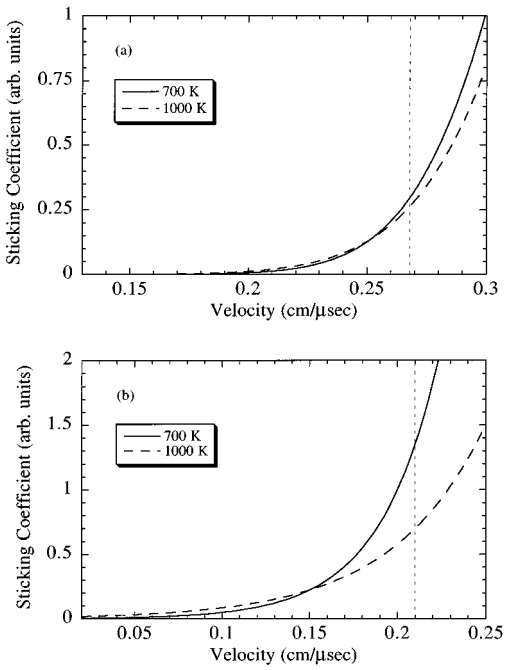

FIG. 11. Panel (a): Dependence of the sticking coefficient via the high energy channel on velocity, calculated for 700 K (solid line) and 1000 K (dashed line). The dashed vertical line marks the top of the velocity range measured at 700 K. Panel (b): Same as (a) for sticking via the low energy channel. As discussed in the text, the normalization of these curves is arbitrary: the absolute values of the sticking coefficients cannot be determined from the data.

scramble the energy among all the modes of the molecule.[73] Thus the dynamics are not expected to be strongly temperature dependent.

Extracting information about the PES from the velocity or energy dependence of the sticking coefficient is more difficult. This system does not obey normal energy scaling, which argues against the dynamics being dominated by an essentially one-dimensional barrier, or a distribution of one dimensional barriers in the entrance channel for N_2 sticking. Total energy scaling, which is observed for the activated channel of N_2 sticking on W(100)[15] and W(110),[13] also fails to describe the data. The fact that the constraint on the total energy is negative, so that energy in non-normal directions actually hinders the reaction, is suggestive of a constrained geometry near the transition state. If, for example, the reaction can occur only in a specific point in the unit cell, velocity parallel to the surface might make it less likely for that condition to be met. In this regard, it is important to remember that the energies of the desorbing molecules are *much* higher than those of the Maxwell–Boltzmann distribution at the surface temperature: Only a few percent have enough energy to overcome the barrier. Thus we may be sampling only the lowest possible barriers at the most optimal geometries, rather than seeing an ''average'' barrier characteristic of a large energy range on the PES.

Surprisal analysis of the low energy peak

Surprisal plots of velocity distributions at 60° were found to be linear for a constraint on the velocity and clearly

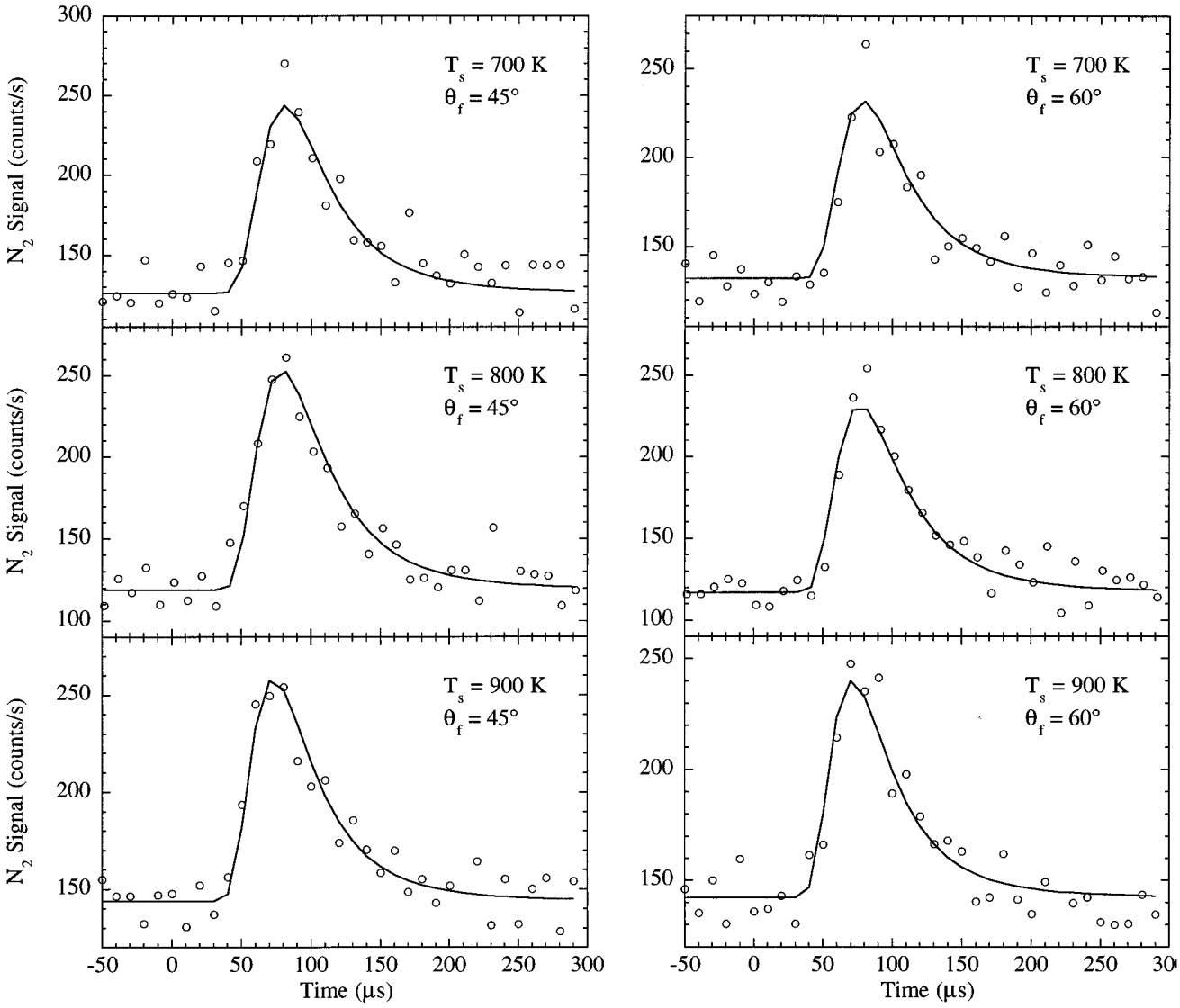

FIG. 12. Fits of the TOF spectra at $\theta_f=45°$ and $\theta_f=60°$ to the surprisal form in Eq. (18).

nonlinear for a constraint on v^2. Since the angular distribution is cosine, there is no constraint on the angle, and the expected form for the velocity distributions is

$$f(v)=Nf_0(v)\exp(\lambda v), \tag{18}$$

where N is a normalization constant, $f_0(v)$ is the prior distribution as defined in Eq. (14) and λ is the surprisal parameter. Fits of the data at 45° and 60° and a few temperatures are shown in Fig. 12. As above, N and λ are not functions of the desorption angle, so a single value of λ is determined for each T_s. The fits are not quite as good as shifted Boltzmanns (which is why the latter were used in fitting the high energy peak) but Eq. (18) describes the data quite well, and with fewer parameters. The temperature dependence of the surprisal parameter is shown in Fig. 13.

As with the high energy peak, and with the same caveats, the surprisal results may be interpreted using detailed balance to extract the velocity dependence of the sticking coefficient for this channel

$$s(v,\theta_f)\propto\exp(\lambda v). \tag{19}$$

Figure 13 shows that λ has a fairly strong temperature dependence. As mentioned earlier, this can be due to temperature dependence of the dynamics or be a result of the different energy ranges probed at different temperatures. The latter idea can be tested, to some extent, by attempting to construct an $s(v,\theta_f)$ function which covers the entire energy range. Panel (b) of Fig. 11 is analogous to panel (a): The solid line is $s(v)$ at 700 K and the dashed line is $s(v)$ at 1000 K, calculated from values of the surprisal parameter from the line fit in Fig. 13. The dashed vertical line marks the top of the energy range of the 700 K data. Again, the absolute values of the sticking coefficients are not known, and the sticking coefficients have been arbitrarily set equal at $v=0.15$ cm/μs. Unlike the case of the high energy peak, the two $s(v)$ curves are substantially different even where the energy ranges of the two measurements overlap, which suggests that the dynamics are actually temperature dependent in this case.

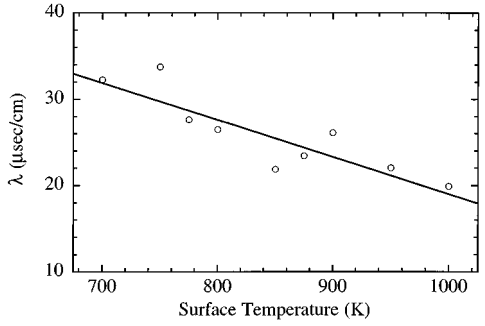

FIG. 13. Temperature dependence of the surprisal parameter used to fit the low energy peak.

Although Fig. 11(b) shows the sticking coefficient at 1000 K to be smaller than at 700 K, this is strictly due to the arbitrary normalization shown: It could actually be larger or smaller.

The data show that the reaction probability (and, equivalently, the sticking coefficient) for this channel is independent of angle, so that it obeys total energy scaling instead of normal energy scaling, and that it is less sensitive to the energy at higher temperatures. These two facts suggest that the molecule interacts strongly with the surface before it desorbs (or sticks) so that the energy becomes scrambled among the modes of the molecule. There may also be some energy exchange with the surface. This would be easiest to understand if the nitrogen molecule were trapped in a molecular chemisorbed state, and there were a barrier between that state and dissociation, as has been suggested for N_2 dissociative chemisorption on Fe(111)[5] and W(110).[13] Another possibility is that the molecule has multiple encounters with a corrugated potential during the reaction.

CONCLUSIONS

We have reported measurements of the velocity distributions of product N_2 molecules formed by the reduction of NO by H_2 on Rh(111) in the low nitrogen coverage limit as a function of surface temperature and desorption angle. The N_2 molecules desorb with average translational energies three to four times that expected for molecules equilibrated at the surface temperature. The angular and velocity distributions are well fit by bimodal forms. The higher energy component has a $\cos^{25}(\Theta_f)$ angular distribution, and its average energy depends on desorption angle. The low energy component is cosine distributed, and its energy is independent of angle. Both channels are substantially hyperthermal.

Surprisal analysis may be applied to both channels. The high energy peak may be fit at all angles at a given surface temperature with two dynamical parameters corresponding to constraints on the normal velocity and the total energy. The strong weighting toward large normal velocities and negative constraint on the total energy may suggest a highly geometrically constrained transition state with a high barrier. The low energy peak may be fit with a single dynamical constraint on the total velocity, and the dynamics of this channel appear to be temperature dependent; these properties of the dynamics both suggest a strong interaction of the molecule with the surface during the reaction.

ACKNOWLEDGMENTS

J.I.C. acknowledges financial support from AT&T Bell Laboratories through the Graduate Research Program for Women. Acknowledgment is made to the donors of The Petroleum Research Fund, administered by the ACS, for partial support of this research. Additional support from the NSF Materials Research Science and Engineering Center at The University of Chicago is also gratefully acknowledged.

[1] W. F. Egelhoff, in *The Chemical Physics of Solid Surfaces and Heterogeneous Catalysis*, edited by D. A. King and D. P. Woodruff (Elsevier, New York, 1982).
[2] K. C. Taylor, *Automobile Catalytic Converters*, (Springer, Berlin, 1984).
[3] R. M. Wolf, J. Siera, F. C. M. J. M. v. Delft, and B. E. Nieuwenhuys. Faraday Discuss. Chem. Soc. **87**, 275 (1989).
[4] L. Bugyi and F. Solymosi, Surf. Sci. **258**, 55 (1991).
[5] R. Raval, M. A. Harrison, and D. A. King, in *The Chemical Physics of Solid Surfaces and Hetergenous Catalysis*, edited by D. A. King and D. P. Woodruff (Elsevier, New York, 1990).
[6] C. T. Rettner and H. Stein, Phys. Rev. Lett. **59**, 2768 (1987).
[7] C. T. Rettner and H. Stein, J. Chem. Phys. **87**, 770 (1987).
[8] R. P. Thorman and S. L. Bernasek, J. Chem. Phys. **74**, 6498 (1981).
[9] G. Haase and M. Asscher, Surf. Sci. **191**, 75 (1987).
[10] G. Haase, M. Asscher, and R. Kosloff, J. Chem. Phys. **90**, 3346 (1989).
[11] G. D. Billing, A. Guldberg, N. E. Henriksen, and F. Y. Hansen, Chem. Phys. **147**, 1 (1990).
[12] N. E. Henriksen, G. D. Billing, and F. Y. Hansen, Surf. Sci. **227**, 224 (1990).
[13] H. E. Pfnür, C. T. Rettner, J. Lee, R. J. Madix, and D. J. Auerbach, J. Chem. Phys. **85**, 7452 (1986).
[14] C. T. Rettner, H. Stein, and E. K. Schweizer, J. Chem. Phys. **89**, 3337 (1988).
[15] C. T. Rettner, E. K. Schweizer, and H. Stein, J. Chem. Phys. **93**, 1442 (1990).
[16] G. Comsa and R. David, Chem. Phys. Lett. **49**, 512 (1977).
[17] G. Comsa and R. David, Surf. Sci. **117**, 77 (1982).
[18] H. A. Michelson, C. T. Rettner, D. J. Auerbach, and R. N. Zare, J. Chem. Phys. **98**, 8294 (1993).
[19] L. K. Verheij, M. B. Hugenschmidt, A. B. Anton, B. Poelsema, and G. Comsa, Surf. Sci. **210**, 1 (1989).
[20] C. A. Becker, J. P. Cowin, L. Wharton, and D. J. Auerbach, J. Chem. Phys. **67**, 3394 (1977).
[21] L. S. Brown and S. J. Sibener, J. Chem. Phys. **90**, 2807 (1989).
[22] T. Matsushima, K. Shobatake, and Y. Ohno, Surf. Sci. **283**, 101 (1993).
[23] Y. Ohno, T. Matsushima, and H. Uetsuka, J. Chem. Phys. **101**, 5319 (1994).
[24] E. Poelmann, M. Schmitt, and H. Hoinkes, Surf. Sci. **287/288**, 269 (1993).
[25] K.-H. Allers, H. Pfnür, P. Feulner, and D. Menzel, J. Chem. Phys. **100**, 3985 (1994).
[26] K.-H. Allers, H. Pfnür, P. Feulener, and D. Menzel, Surf. Sci. **291**, 167 (1993).
[27] J. I. Colonell, K. D. Gibson, and S. J. Sibener, J. Chem. Phys. **103**, 6677 (1995).
[28] K. D. Gibson, J. I. Colonell, and S. J. Sibener, J. Chem. Phys. **103**, 6735 (1995).
[29] K. D. Gibson, J. I. Colonell, and S. J. Sibener, Surf. Sci. Lett. **343**, L1151 (1995).
[30] G. Comsa and R. David, Surf. Sci. Rep. **5**, 145 (1985).
[31] K. D. Gibson and S. J. Sibener, J. Chem. Phys. **88**, 7862 (1988).
[32] D. F. Padowitz and S. J. Sibener, Surf. Sci. **254**, 125 (1991).
[33] D. Bassi, in *Atomic and Molecular Beam Methods*, Vol. I, edited by G. Scoles (Oxford University, New York, 1988).
[34] L. Bugyi and F. Solymosi, Surf. Sci. **188**, 475 (1987).
[35] J. T. Yates, P. A. Thiel, and W. H. Weinberg, Surf. Sci. **84**, 427 (1979).
[36] T. W. Root, L. D. Schmidt, and G. B. Fisher, Surf. Sci. **134**, 30 (1983).
[37] D. J. Auerbach, C. T. Rettner, and H. A. Michelson, Surf. Sci. **283**, 1 (1993).

[38] C. T. Rettner, D. J. Auerbach, and H. A. Michelson, J. Vac. Sci. Technol. A **10**, 2282 (1992).
[39] J. Segner, C. T. Campbell, G. Doyen, and G. Ertl, Surf. Sci. **138**, 505 (1984).
[40] H. H. Sawin and R. P. Merrill, J. Chem. Phys. **73**, 996 (1980).
[41] V. A. Ukraintsev and I. Harrison, J. Chem. Phys. **98**, 5971 (1993).
[42] L. Bugyi, J. Kiss, K. Révész, and F. Solymosi, Surf. Sci. **233**, 1 (1990).
[43] C. T. Campbell and J. M. White, Appl. Surf. Sci. **1**, 347 (1978).
[44] L. A. DeLouise and N. Winograd, Surf. Sci. **159**, 199 (1985).
[45] H. A. C. M. Hendrickx and B. E. Niuwenhuys, Surf. Sci. **175**, 185 (1985).
[46] C.-T. Kao, G. S. Blackman, M. A. V. Hove, and G. A. Somorjai, Surf. Sci. **224**, 77 (1989).
[47] T. W. Root, G. B. Fisher, and L. D. Schmidt, J. Chem. Phys. **85**, 4679 (1986).
[48] T. W. Root, G. B. Fisher, and L. D. Schmidt, J. Chem. Phys. **85**, 4687 (1986).
[49] D. N. Belton and S. J. Schmieg, J. Catal. **144**, 9 (1993).
[50] W. C. Hecker and A. T. Bell, J. Catal. **92**, 247 (1985).
[51] F. Mertens and R. Imbihl, Nature (London) **370**, 124 (1994).
[52] A. Obuchi, S. Naito, T. Onishi, and K. Tamaru, Surf. Sci. **130**, 29 (1983).
[53] S. H. Oh, G. B. Fisher, J. E. Carpenter, and D. W. Goodman, J. Catal. **100**, 360 (1985).
[54] T. W. Root, L. D. Schmidt, and G. B. Fisher, Surf. Sci. **130**, 173 (1985).
[55] J. Siera, P. Cobden, K. Tanaka, and B. E. Nieuwenhuys, Catal. Lett. **10**, 335 (1991).
[56] M. F. H. v. Tol, A. Gielbert, and B. E. Nieuwenhuys, Catal. Lett. **16**, 297 (1992).
[57] M. F. H. v. Tol, P. T. Wouda, and B. E. Nieuwenhuys, J. Vac. Sci. Technol. A **12**, 2176 (1994).
[58] H. Hirano, T. Yamada, K. I. Tanaka, J. Siera, P. Cobden, and B. E. Nieuwenhuys, Surf. Sci. **262**, 97 (1992).
[59] J. Siera, B. E. Nieuwenhuys, H. Hirano, T. Yamada, and K. I. Tanaka, Catal. Lett. **3**, 179 (1989).
[60] K. I. Tanaka, T. Yamada, and B. E. Nieuwenhuys, Surf. Sci. **242**, 503 (1991).
[61] H. A. C. M. Hendrickx, A. Hoek, and B. E. Nieuwenhuys, Surf. Sci. **135**, 81 (1983).
[62] W. van Willigen, Phys. Lett. A **28**, 80 (1968).
[63] G. Doyen, Vacuum **32**, 91 (1982).
[64] G. Anger, A. Winkler, and K. D. Rendulic, Surf. Sci. **220**, 1 (1989).
[65] R. D. Levine and R. B. Bernstein, *Molecular Reaction Dynamics and Chemical Reactivity*, (Oxford University, New York, 1987).
[66] B. Halpern and M. Kori, Chem. Phys. Lett. **138**, 261 (1987).
[67] M. Kori and B. Halpern, Chem. Phys. Lett. **129**, 407 (1986).
[68] R. D. Levine, Ann. Rev. Phys. Chem. **29**, 59 (1978).
[69] R. D. Levine and J. L. Kinsey, in *Atom–Molecule Collision Theory: A Guide for the Experimentalist*, edited by R. B. Bernstein (Plenum, New York, 1978).
[70] M. B. Faist, R. D. Levine, and R. B. Bernstein, J. Chem. Phys. **66**, 511 (1977).
[71] E. Pollak and R. D. Levine, Chem. Phys. **21**, 61 (1977).
[72] J. I. Steinfeld, J. S. Francisco, and W. L. Hase, *Chemical Kinetics and Dynamics* (Prentiss Hall, Englewood Cliffs, 1989).
[73] A. E. Depristo and A. Kara, Adv. Chem. Phys. **77**, 163 (1990).